Self-Powered Photoelectrochemical Biosensor Based on CdS/RGO/ZnO Nanowire Array Heterostructure

*Kun Zhao, Xiaoqin Yan, Yousong Gu, Zhuo Kang, Zhiming Bai, Shiyao Cao, Yichong Liu, Xiaohui Zhang, and Yue Zhang**

***A** CdS/reduced graphene oxide (RGO)/ZnO nanowire array (NWAs) heterostructure is designed, which exhibits enhanced photoelectrochemical (PEC) activity compared to pure ZnO, RGO/ZnO, and CdS/ZnO. The enhancement can be attributed to the synergistic effect of the high electron mobility of ordered 1D ZnO NWAs, extended visible-light absorption of CdS nanocrystals, and the formed type II band alignment between them. Moreover, the incorporation of RGO further promotes the charge carrier separation and transfer process due to its excellent charge collection and shuttling characteristics. Subsequently, the CdS/RGO/ZnO heterostructure is successfully utilized for the PEC bioanalysis of glutathione at 0 V (vs Ag/AgCl). The self-powered device demonstrates satisfactory sensing performance with rapid response, a wide detection range from 0.05 mM to 1 mM, an acceptable detection limit of 10 μM, as well as certain selectivity, reproducibility, and stability. Therefore, the CdS/RGO/ZnO heterostructure has opened up a promising channel for the development of PEC biosensors.*

1. Introduction

Photoelectrochemical (PEC) bioanalysis, a newly emerging and promising technique, has provoked considerable interest and developed at a dramatically fast rate. Due to the complete separation of excitation source and detection signal, the background noise of PEC sensors decreases dramatically, contributing to a higher sensitivity compared with conventional electrochemical and optical methods.[1] Besides, the simple detection equipment, fast response, and low cost also make PEC bioanalysis a competitive avenue for biodetection. Moreover, some PEC biosensors can even work without extra voltage, avoiding the interference of other biomolecules. For example, graphene–CdS composites[2] and ZnO/ reduced graphene oxide (RGO) hybrid system[3] were employed to detect glutathione (GSH) without applying external potential. Therefore, enormous efforts have been devoted to the development of PEC sensors by combining several functional materials. For instance, quantum-dot sensitized structures, such as Au–SnO_2/CdS nanocomposite,[4] CdS/ZnO nanospheres,[5] and ZnS/CdTe/Mn–CdS/ZnS sensitized ZnO nanosheets,[6] were employed to obtain PEC sensors with excellent sensitivity and selectivity. Then p–n heterostructures such as the flower-like Cu_2O/ZnO[7] and poly(3-hexylthiophene) modified TiO_2 nanoparticles[8] were also adopted to enhance the sensing performance. Furthermore, other hybrid systems, including glucose oxidase functionalized TiO_2 nanowires,[9] IrO_2–hemin–TiO_2 nanowire arrays (NWAs),[10] and $Cd_{0.5}Zn_{0.5}S$–RGO nanocomposite,[11] were applied in PEC sensors. Even though some progress has been made in PEC bioanalysis, it remains a big challenge

K. Zhao, Prof. X. Yan, Prof. Y. Gu, Z. Kang, Z. Bai, S. Cao, Y. Liu, X. Zhang, Prof. Y. Zhang
State Key Laboratory for Advanced Metals and Materials
School of Materials Science and Engineering
University of Science and Technology Beijing
Beijing 100083, China
E-mail: yuezhang@ustb.edu.cn
Prof. Y. Zhang
Key Laboratory of New Energy Materials and Technologies
University of Science and Technology Beijing
Beijing 100083, China

DOI: 10.1002/smll.201502042

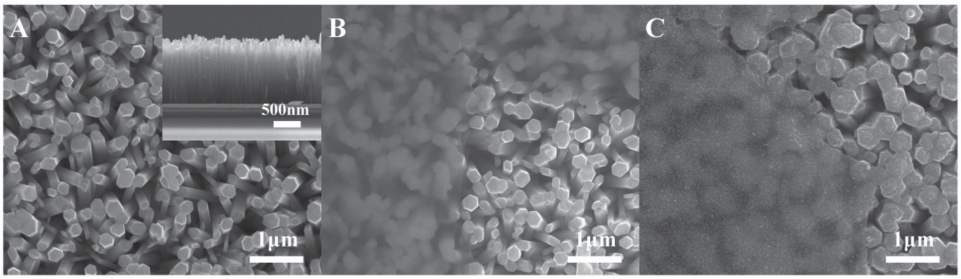

Figure 1. The FESEM images of A) pure ZnO NWAs; the inset shows the cross-sectional image of ZnO NWs; B) RGO/ZnO; C) CdS/RGO/ZnO heterostructure.

to develop new structures for high-performance PEC biosensors.

Since photoactive material is a critical factor influencing the performance of PEC sensors, the perfect design of photoelectrode material has become the main focus of PEC research. Generally, aligned 1D nanomaterials have been widely used in PEC devices[12–21] because they possess large surface-to-volume ratios and can provide direct pathway for carrier transport through the axial lengths, thus inhibiting the recombination of charge carriers and enhancing the PEC activity. Among them, ZnO NWAs have been extensively investigated because of their high electron mobility and well-controlled morphology.[22–25] However, the wide bandgap (3.37 eV) of ZnO has restricted its light absorption to ultraviolet range, which accounts for only a small portion of sunlight. One solution to this problem is to decorate 1D ZnO nanomaterials with narrow bandgap semiconductors, such as CdS,[15–17] CdSe,[18,19] and CdTe.[20,21] Among various sensitizers, CdS with a band gap of 2.4 eV is frequently adopted to extend the absorption range of ZnO due to its exceptional visible-light absorption ability and facile synthesis. Besides, a type II alignment can be formed between CdS and ZnO,[26] facilitating the electron injection from CdS to ZnO and further suppressing the recombination of photogenerated electron–hole pairs. Noticeably, due to its excellent electron mobility and high specific surface area,[27–29] graphene (GR) or its derivative RGO has been frequently introduced to further boost the PEC activity where GR works as an electron mediator to promote the charge separation efficiency.[30–32]

In this work, we designed a CdS/RGO/ZnO heterostructure to take advantage of the preeminent charge transport characteristics of aligned 1D ZnO NWAs, the remarkable visible-light absorption ability of CdS, and the marvelous charge collection and shuttling property of RGO. In contrast to the pure ZnO, RGO/ZnO, and CdS/ZnO, the CdS/RGO/ZnO heterostructure demonstrated the supreme PEC activity, exhibiting the lowest charge transfer resistance and the highest photocurrent density at 0 V (vs Ag/AgCl). Therefore, we applied this heterostructure in the PEC bioanalysis of GSH, an important cellular thiol in many biological functions involving antioxidant defense, signal transduction, and cell proliferation.[33] The device demonstrated self-powered ability, rapid response, wide linear detection range, certain selectivity, and stability, suggesting its encouraging promise in the application of PEC biosensors.

2. Results and Discussion

2.1. Characterization of the As-Prepared Samples

The field emission scanning electron microscopic (FESEM) images of different structures are displayed in **Figure 1**. It can be seen that ZnO NWAs were grown vertically and uniformly on the fluorine-doped tin oxide (FTO) glass with an average diameter of 200 nm and a length of about 3 μm (Figure 1A). After the introduction of RGO, a smooth layer of RGO was observed on top of the ZnO NWAs (Figure 1B). It is worthwhile to note that the RGO layer is thin enough to see the ZnO NWAs under it, indicating the interlayer will not seriously affect the absorption of light. Both the RGO layer and the ZnO NWAs became rough as shown in Figure 1C, the evidence of the successful decoration of CdS. Obviously, the CdS nanocrystals were evenly distributed on the RGO layer and the ZnO NWAs. The transmission electron microscopy (TEM) image in Figure S1A (Supporting Information) further confirmed the uniform distribution of CdS on ZnO NWAs and the HRTEM image in Figure S1B (Supporting Information) revealed that the ZnO nanowires grew along the *c*-axis with CdS nanocrystals, whose lattice spacings of 0.33 and 0.31 nm can be assigned to the (002) and (101) planes, respectively.

The main component elements of Cd, S, Zn, and O in the CdS/RGO/ZnO heterostructure were characterized by the full X-ray photoelectron spectroscopy (XPS) spectrum (**Figure 2**A). The high-resolution spectrum of Cd 3d (Figure 2B) with peaks at 405.7 eV (Cd $3d_{5/2}$) and 412.5 eV (Cd $3d_{3/2}$) confirms the existence of Cd^{2+}.[15] The peaks at 161.9 eV (S $2p_{3/2}$) and 163.1 eV (S $2p_{1/2}$) in Figure 2C are indicative of S^{2-} in CdS.[34] Besides, the molar ratio of Cd and S is calculated to be about 1:1, which matches well with the stoichiometric ratio of CdS.

To investigate the reduction degree of graphene oxide (GO), high-resolution XPS spectra of C 1s were collected from GO/ZnO and CdS/RGO/ZnO. The C 1s spectrum of GO/ZnO (Figure 2D, solid line) can be divided into four distinct peaks, which were located at 284.80, 286.75, 287.50, and 288.60 eV corresponding to C—C, C—O, C=O and O=C—OH, respectively.[35] In contrast, in the XPS C 1s spectrum of CdS/RGO/ZnO (Figure 2E), the peak for C=O almost vanished while the intensity of peaks for C—O and O=C—OH decreased dramatically, demonstrating the partial removal of oxygen-containing functional groups and

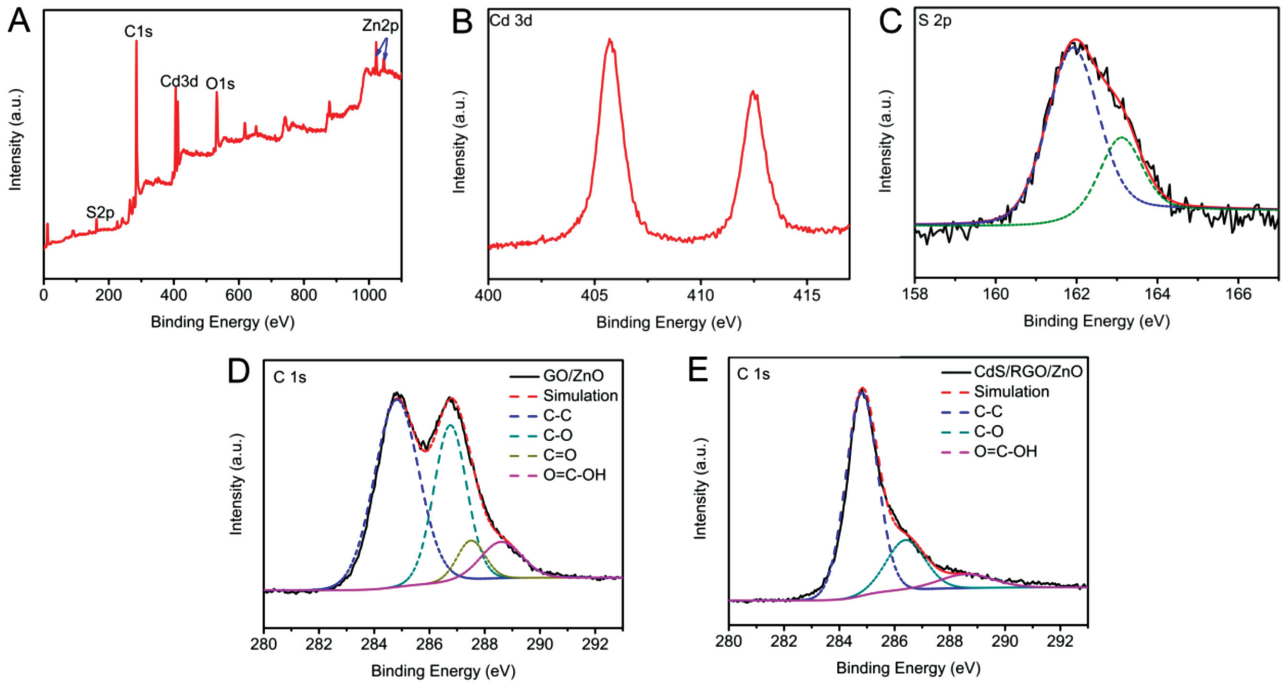

Figure 2. A) Full XPS spectrum of CdS/RGO/ZnO; B) high-resolution XPS spectra of Cd 3d and C) S 2p; (D) C 1s for GO/ZnO; E) C 1s for CdS/RGO/ZnO.

the partial reduction of GO. Fourier transform infrared (FTIR) spectra were utilized to further confirm the reduction of GO. It is shown in **Figure 3**A (red line) that the distinctive bands of GO appeared at 1075 (C—O stretching), 1263 (C—OH stretching), 1623 (C=C), 1721 (C=O stretching), and 1418, 3319 cm^{-1} (O—H stretching), indicative of the existence of various oxygen-containing functional groups in GO.[36,37] When GO was reduced to RGO via a photochemical method, all these absorption bands either disappeared or had a significant decrease in absorption intensity (Figure 3A, blue line). Meanwhile, a new absorption band at 1550 cm^{-1} emerged, which is the unique skeletal vibration of GR and can be assigned to the restoration of sp^2 hybrid carbon skeleton after photochemical reduction.[34,38] The result of FTIR is consistent with that of XPS, both of which substantiate the reduction of GO.

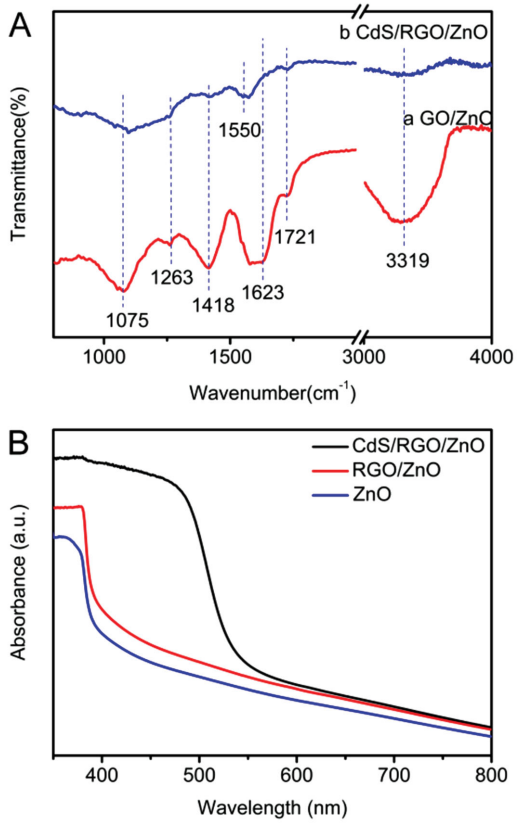

Figure 3. A) FTIR spectra of a) GO/ZnO and b) CdS/RGO/ZnO; B) UV–vis absorption spectra of ZnO, RGO/ZnO, and CdS/RGO/ZnO.

The optical absorption property of various modified electrodes was characterized by the UV–visible (UV–vis) absorption spectra. As illustrated in Figure 3B, the absorption edge of pure ZnO is about 380 nm, which is in accord with its bandgap. After coupled with RGO, the composite RGO/ZnO exhibited the similar absorption edge to pure ZnO with a slightly higher absorbance owing to the absorption of RGO itself.[32] The ternary composite CdS/RGO/ZnO displayed the highest absorption ability and its absorption range was extended to the visible light because of the decoration of CdS.

2.2. Photoelectrochemical Property of the CdS/RGO/ZnO Photoelectrode

Electrochemical impedance spectroscopy (EIS) is a valuable tool to characterize the interfacial charge transfer on the electrode. The diameter of the semicircle in a Nyquist plot can represent the interfacial charge transfer resistance (R_{ct}). The samples revealed lower R_{ct} under illumination than in the dark (**Figure 4**), suggesting the fast interfacial charge

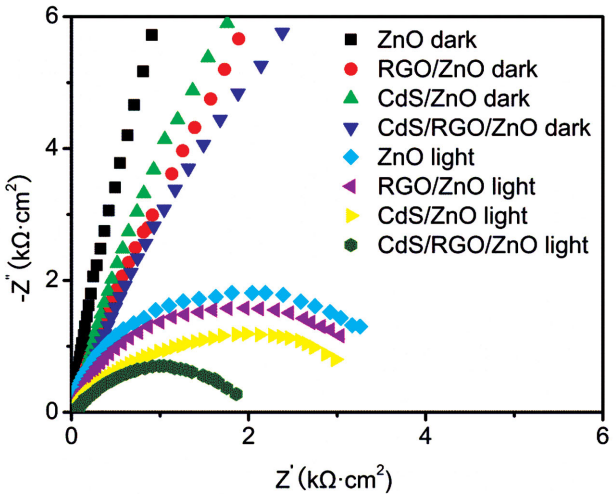

Figure 4. EIS Nyquist plots of ZnO, RGO/ZnO, CdS/ZnO, and CdS/RGO/ZnO in the dark and under illumination in 0.1 M PBS (pH = 7.4).

transfer upon illumination. It is noticeable that the CdS/RGO/ZnO electrode exhibited the lowest R_{ct}, illustrating the most efficient charge separation and transfer process. This can be ascribed to the synergetic effect of the three materials. The diameter of CdS/ZnO has become smaller than that of pure ZnO, proving that the decoration of CdS has facilitated the charge transfer process due to the type II band alignment between ZnO and CdS. The smaller R_{ct} of CdS/RGO/ZnO than that of CdS/ZnO implies that RGO has played an important role in promoting the charge separation and transfer.

The photocurrent measurements were conducted to assess the potential of the CdS/RGO/ZnO heterostructure as a PEC biosensor. First, the *I–V* characteristics of various photoelectrodes were tested from –0.7 to 1 V (vs Ag/AgCl) (**Figure 5**A). The photocurrent density of the CdS/RGO/ZnO heterostructure at 0 V (vs Ag/AgCl) was highest compared to pure ZnO, RGO/ZnO, and CdS/ZnO. Second, the transient photocurrent response of different modified electrodes was studied at 0 V (vs Ag/AgCl) under simulated sunlight illumination (Figure 5B). Under illumination, a rapid photocurrent response was observed for all the modified electrodes. The CdS/RGO/ZnO modified electrode showed the highest photocurrent density of 0.18 mA cm^{-2} (curve d). The CdS/ZnO heterostructure possessed higher photocurrent density than pure ZnO due to the excellent visible-light absorption ability of CdS and the step-like band alignment between ZnO and CdS. Moreover, the higher photocurrent density of CdS/RGO/ZnO than that of CdS/ZnO (curve c) demonstrated the efficient separation of photogenerated electron–hole pairs because of the introduction of RGO as an effective electron acceptor and transport channel. The enhancement of the CdS/RGO/ZnO heterostructure can be explained in **Scheme 1**. Under irradiation, both ZnO and CdS can be excited to generate electron–hole pairs. Due to the type II alignment between ZnO and CdS, the photogenerated electron–hole pairs can be efficiently separated.[26] The excited electrons on the conduction band (CB) of CdS are favorably injected to the CB of ZnO, which subsequently transfer to the FTO substrate, while the excited holes on

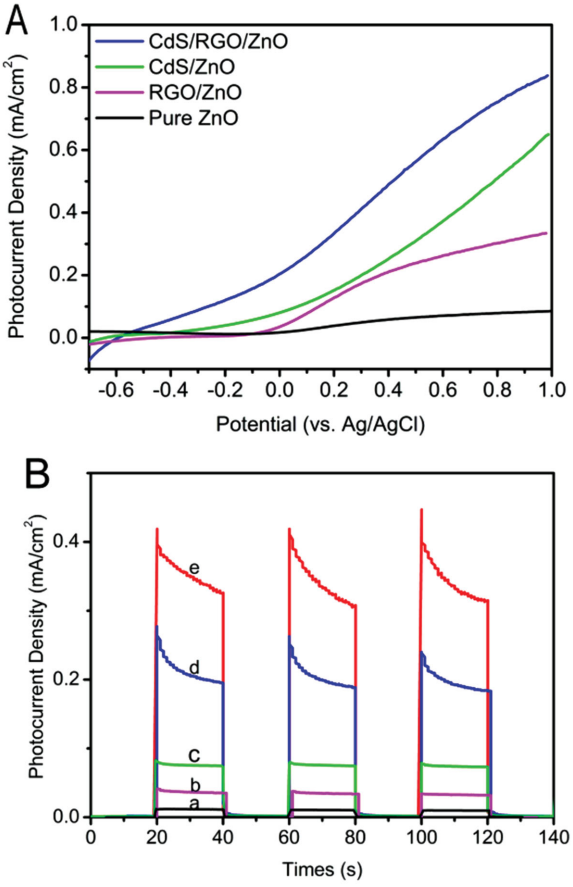

Figure 5. A) *I–V* curves of pure ZnO, RGO/ZnO, CdS/ZnO, CdS/RGO/ZnO under illumination in 0.1 M PBS (pH = 7.4); B) photocurrent response of a) ZnO, b) RGO/ZnO, c) CdS/ZnO, d) CdS/RGO/ZnO in 0.1 M PBS (pH = 7.4), and e) CdS/RGO/ZnO in 0.1 M PBS (pH = 7.4) containing 400 μM GSH at zero bias under illumination.

the valence band (VB) of ZnO flow favorably to the VB of CdS. Besides, RGO can facilitate the transfer process of the excited electrons on the CB of CdS to ZnO because of its superior charge collection and shuttle characteristics.[39] Upon addition of 400 μM GSH, the photocurrent density went up to 0.30 mA cm^{-2} (curve e), which can be explained as follows: GSH was oxidized by the photogenerated holes in CdS and therefore effectively obstructed the recombination of the photogenerated electron–hole pairs, resulting in a considerable increase of the photocurrent density. All the PEC measurements provided evidence that the CdS/RGO/ZnO heterostructure possessed an enhanced PEC activity due to the synergistic effect of CdS, RGO, and ZnO, guaranteeing the possibility of its subsequent application in PEC detection.

2.3. Photoelectrochemical Detection of GSH

With the increasing concentration of GSH, more photoexcited holes on the VB of CdS are consumed to oxidize GSH. Thus, the consumption of the photoexcited holes contributed to more efficient separation of photogenerated charge carries, leading to an increment in the photocurrent. In order to avoid the interference of other biomolecules, 0 V was chosen

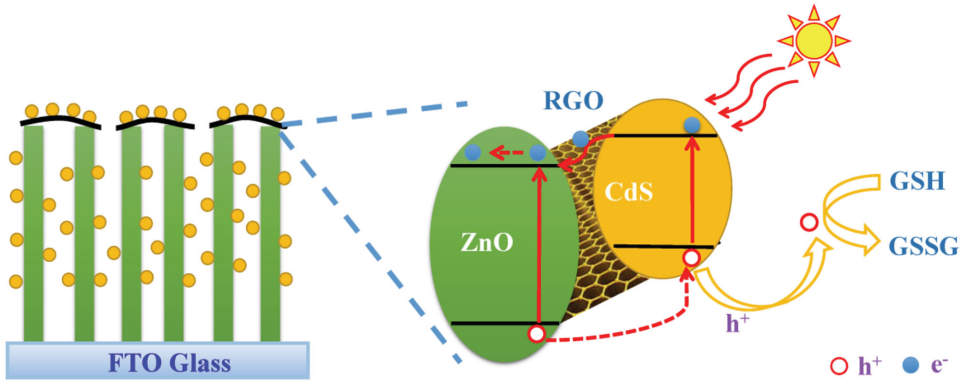

Scheme 1. Schematic illustration of the mechanism for the PEC detection of GSH.

as the work potential. The response of the CdS/RGO/ZnO electrode to GSH was investigated via the time-dependent current measurement under simulated sunlight illumination (**Figure 6**A). An excellent linear relationship (R^2 = 0.9986) was acquired between the photocurrent density and the concentration of GSH (**Figure 7**B). The PEC biosensor displayed a linear range from 0.05 to 1 mM with a detection limit of 10 μM (at a signal-to-noise ratio of 3). The linear range of our device was wider than those obtained by the surface-enhanced Raman scattering method (0.1–0.8 μM),[40] the electrogenerated chemiluminescence method of quantum dots (24–214 μM)[41] and other PEC methods.[3,7,42] Although the detection limit of our biosensor was a bit higher than those in previous reports,[2,41] its upper detection limit of 1 mM was more appropriate to detect GSH in biological samples since the intracellular GSH concentration in most mammalian cells varies from 1 to 10 mM.[43] Likewise, the CdS/RGO/ZnO biosensor can work without extra applied voltage and respond fast to the addition of GSH. Consequently, the proposed PEC biosensor holds great potential for the practical application in the future.

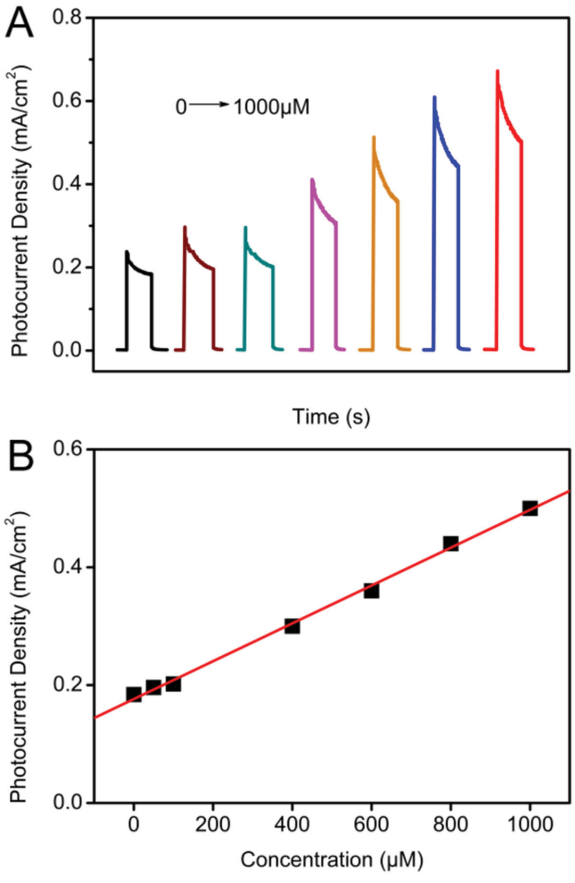

Figure 6. A) Photocurrent response of the CdS/RGO/ZnO electrode in 0.1 M PBS (pH = 7.4) in the presence of 0, 50, 100, 400, 600, 800, and 1000 μM GSH (from left to right) at 0 V (vs Ag/AgCl) under simulated sunlight illumination. B) Linear relationship between photocurrent density and GSH concentration.

2.4. Selectivity, Reproducibility, and Stability

The selectivity is a critical aspect in the application of biosensors. Therefore, the influence of different biological species on the photocurrent response of the CdS/RGO/ZnO electrode was studied to confirm the selectivity of our device. As Figure 7 shows, no salient photocurrent change was observed with the successive addition of 50 μM glucose, ascorbic acid (AA), bovine serum albumin (BSA), lactic acid (LA), uric acid (UA), and dopamine (DA) into the electrolyte containing 200 μM GSH. The result indicated that these biomolecules had negligible influence on the detection of GSH. Furthermore, the device possessed satisfactory reproducibility with the relative standard deviation of 4.4% and 5.1% for five successive measurements of the photocurrent density with the GSH concentration of 50 and 100 μM, respectively. Eventually, the stability of the biosensor was verified via the intermittent photocurrent response tests. About 98% of the initial photocurrent was obtained 3 d later and 92.4% of the initial photocurrent was maintained after 1 week.

3. Conclusion

In summary, we successfully developed a PEC biosensor for the self-powered detection of GSH using the CdS/RGO/ZnO NWAs heterostructure. Aligned 1D ZnO NWAs provided a direct channel for charge transfer, CdS nanocrystals increased the visible-light absorption and the type II alignment between them facilitated the separation of

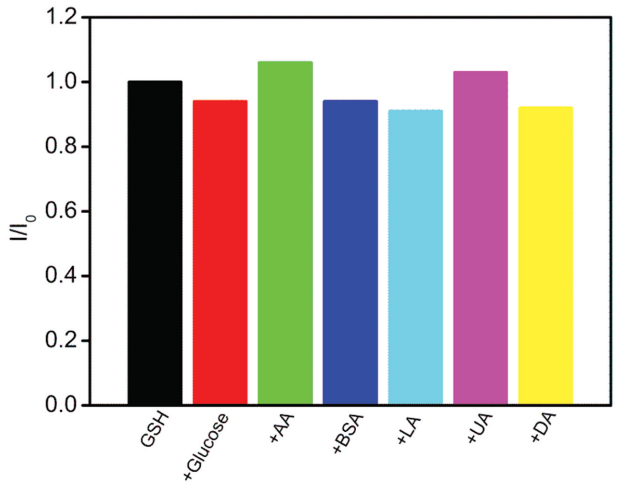

Figure 7. Photocurrent ratio I/I_0 of the CdS/RGO/ZnO electrode in 0.1 M PBS (pH = 7.4) containing 200 μM GSH with the successive addition of other biomolecules at 0 V (vs Ag/AgCl) under simulated sunlight illumination. The concentration of all other biomolecules is 50 μM. (I and I_0 are photocurrents before and after the addition of other interferents, respectively).

photoexcited charge carriers. Furthermore, the marvelous charge collection and shuttle characteristics of RGO also contributed to the efficient separation of photogenerated electron–hole pairs. Afterward, the self-powered biosensor demonstrated satisfactory sensing performance, with a wide detection linear range from 0.05 to 1 mM and an acceptable detection limit of 10 μM, along with certain selectivity, reproducibility, and stability. These results suggested that the CdS/RGO/ZnO heterostructure can be a competitive candidate in the development of PEC biosensors.

4. Experimental Section

Synthesis of ZnO NWAs: ZnO NWAs were synthesized on FTO glass via a hydrothermal process. First, the FTO substrates were spin-coated with 0.25 M zinc acetate in a solution of 2-methoxyethanol and monoethanolamine to form a seed layer of ZnO, followed by heat treatment at 350 °C for 30 min. Then the seeded FTO substrates were immersed in an aqueous solution of 0.05 M zinc nitrate ($Zn(NO_3)_2{\cdot}6H_2O$) and 0.05 M hexamethylenetetramine and kept at 95 °C for 12 h. After naturally cooling down to room temperature, the ZnO NWAs-coated substrates were removed from the solution, rinsed with deionized (DI) water, and then dried in air.

Formation of RGO/ZnO: Graphene oxide solution was purchased from Tianjin Plan Nano Technology Co. Ltd. The concentration of the GO solution is 0.5 mg mL^{-1}. The GO solution was spin-coated on the ZnO NWAs. Then the ZnO/GO was annealed at 500 °C for 2 h in an argon atmosphere. RGO was obtained via photocatalytic reduction according to the previous literature.[30,44] Namely, ZnO/GO was immersed in ethanol and then irradiated under UV light (λ = 313 nm) for 2 h to reduce GO. Finally, the obtained ZnO/RGO was washed with DI water and dried in air.

Fabrication of CdS/RGO/ZnO: CdS was deposited on ZnO/RGO via the nanocrystal layer deposition method.[45] ZnO/RGO was incubated in an aqueous solution of 0.02 M cadmium nitrate ($Cd(NO_3)_2{\cdot}4H_2O$) and 0.02 M thioacetamide at 40 ° C for 10 min. Then the substrate was removed from the solution, washed with DI water, and dried in air.

Characterization of the Samples: The morphologies of the hybrids were characterized using FESEM (QUANTA 3D, FEI). The structure of the samples was obtained via TEM (Tecnai F30, FEI). X-ray diffraction patterns were carried out on a Rigaku TTRIII X-ray diffractometer using Cu Kα radiation source (λ = 1.54056 Å) to determine the crystal phase of the obtained samples. X-ray photoelectron spectroscopy measurement was conducted on a Kratos AXIS Ultra^{DLD} photoelectron spectrometer with a monochromatic Al Kα source ($h\nu$ = 1486.6 eV). All of the binding energies were calibrated with a reference to the C 1s peak at 284.80 eV. The UV–vis absorption spectra were performed on a Varian Cary 500 Scan UV–vis–NIR spectrometer. Fourier transform infrared spectra were performed on a Varian Excalibur 3100 FTIR spectrophotometer in a frequency range between 800 and 4000 cm^{-1} at a resolution of 0.20 cm^{-1}.

PEC Measurements: All PEC performances were assessed on an electrochemical workstation (Solartron SI1287/SI 1260) in a standard three-electrode system under simulated AM 1.5 G solar light irradiation with a power density of 100 mW cm^{-2} (91159 A, Oriel). In the system, the as-prepared samples served as the working electrode, a Pt wire as the counter electrode and an Ag/AgCl as the reference electrode. 0.1 M phosphate buffer solution (PBS, pH = 7.4) was used as electrolyte. The fabrication procedure of the working electrode was as follows: copper wires were attached to the bare parts of FTO glass with high-purity silver paste and then acrylate glue was used to cover the FTO substrate, the silver paste, and the copper wires to avoid short current in the measurement, leaving an active area of ≈0.1 cm^2. Electrochemical impedance spectroscopy was carried out at 0 V (vs Ag/AgCl) with a frequency range between 100 kHz and 0.1 Hz and an AC amplitude of 5 mV.

Supporting Information

Supporting Information is available from the Wiley Online Library or from the author.

Acknowledgements

This work was supported by the National Major Research Program of China (2013CB932601), the Major Project of International Cooperation and Exchanges (2012DFA50990), the Program of Introducing Talents of Discipline to Universities (B14003), NSFC (51232001, 51172022, 51372023, and 51372020), the Research Fund of Co-construction Program from Beijing Municipal Commission of Education, the Fundamental Research Funds for the Central Universities, and the Program for Changjiang Scholars and Innovative Research Team in University.

[1] Z. Yue, F. Lisdat, W. J. Parak, S. G. Hickey, L. P. Tu, N. Sabir, D. Dorfs, N. C. Bigall, *ACS Appl. Mater. Interfaces* **2013**, *5*, 2800.
[2] X. Zhao, S. Zhou, Q. Shen, L. Jiang, J. Zhu, *Analyst* **2012**, *137*, 3697.

[3] Z. Kang, Y. S. Gu, X. Q. Yan, Z. M. Bai, Y. C. Liu, S. Liu, X. H. Zhang, Z. Zhang, X. J. Zhang, Y. Zhang, *Biosens. Bioelectron.* **2015**, *64*, 499.
[4] Q. M. Shen, J. Y. Jiang, S. L. Liu, L. Han, X. H. Fan, M. X. Fan, Q. L. Fan, L. H. Wang, W. Huang, *Nanoscale* **2014**, *6*, 6315.
[5] Q. Shen, X. Zhao, S. Zhou, W. Hou, J. Zhu, *J. Phys. Chem. C* **2011**, *115*, 17958.
[6] R. Wang, K. Yan, F. Wang, J. Zhang, *Electrochim. Acta* **2014**, *121*, 102.
[7] J. Li, H. Li, Y. Xue, H. Fang, W. Wang, *Sens. Actuators B* **2014**, *191*, 619.
[8] H. B. Li, J. Li, Q. Xu, X. Y. Hu, *Anal. Chem.* **2011**, *83*, 9681.
[9] J. Tang, Y. Wang, J. Li, P. Da, J. Geng, G. Zheng, *J. Mater. Chem. A* **2014**, *2*, 6153.
[10] J. Tang, B. Kong, Y. C. Wang, M. Xu, Y. L. Wang, H. Wu, G. F. Zheng, *Nano Lett.* **2013**, *13*, 5350.
[11] Q. Liu, J. Cai, J. Huan, X. Dong, C. Wang, B. Qiu, K. Wang, *Analyst* **2014**, *139*, 1121.
[12] Q. Huang, F. Kang, H. Liu, Q. Li, X. D. Xiao, *J. Mater. Chem. A* **2013**, *1*, 2418.
[13] J. G. Hou, Z. Wang, C. Yang, H. J. Cheng, S. Q. Jiao, H. M. Zhu, *Energy Environ. Sci.* **2013**, *6*, 3322.
[14] Z. Bai, X. Yan, Z. Kang, Y. Hu, X. Zhang, Y. Zhang, *Nano Energy* **2014**, *14*, 392
[15] W. Sheng, B. Sun, T. Shi, X. Tan, Z. Peng, G. Liao, *ACS Nano* **2014**, *8*, 7163.
[16] G. M. Wang, X. Y. Yang, F. Qian, J. Z. Zhang, Y. Li, *Nano Lett.* **2010**, *10*, 1088.
[17] Y. Tak, S. J. Hong, J. S. Lee, K. Yong, *J. Mater. Chem.* **2009**, *19*, 5945.
[18] K. S. Leschkies, R. Divakar, J. Basu, E. E. Pommer, J. E. Boercker, C. B. Carter, U. R. Kortshagen, D. J. Norris, E. S. Aydil, *Nano Lett.* **2007**, *7*, 1793.
[19] N. Chouhan, C. L. Yeh, S. F. Hu, R. S. Liu, W. S. Chang, K. H. Chen, *Chem. Commun.* **2011**, *47*, 3493.
[20] G. Zhang, S. Jiang, Y. Lin, W. Ren, H. Cai, Y. Wu, Q. Zhang, N. Pan, Y. Luo, X. Wang, *J. Mater. Chem. A* **2014**, *2*, 5675.
[21] C. K. Chen, H. M. Chen, C. J. Chen, R. S. Liu, *Chem. Commun.* **2013**, *49*, 7917.
[22] Y. Zhang, X. Yan, Y. Yang, Y. Huang, Q. Liao, J. Qi, *Adv. Mater.* **2012**, *24*, 4647.
[23] K. Žídek, K. Zheng, C. S. Ponseca, M. E. Messing, L. R. Wallenberg, P. Chábera, M. Abdellah, V. Sundström, T. Pullerits, *J. Am. Chem. Soc.* **2012**, *134*, 12110.
[24] Y. Liu, Y. Gu, X. Yan, Z. Kang, S. Lu, Y. Sun, Y. Zhang, *Nano Res.* **2015**, *8*, 2891.
[25] Z. Kang, X. Yan, Y. Wang, Z. Bai, Y. Liu, Z. Zhang, P. Lin, X. Zhang, H. Yuan, X. Zhang, Y. Zhang, *Sci. Rep.* **2015**, *5*, 7882.
[26] R. Marschall, *Adv. Funct. Mater.* **2014**, *24*, 2421.
[27] S. J. Guo, S. J. Dong, *J. Mater. Chem.* **2011**, *21*, 18503.
[28] X. Zhang, Y. Zhang, Q. Liao, Y. Song, S. Ma, *Small* **2013**, *9*, 4045.
[29] X. Zhang, Q. Liao, M. Chu, S. Liu, Y. Zhang, *Biosens. Bioelectron.* **2014**, *52*, 281.
[30] Y. J. Wang, F. M. Wang, J. He, *Nanoscale* **2013**, *5*, 11291.
[31] W. J. Han, L. Ren, X. Qi, Y. D. Liu, X. L. Wei, Z. Y. Huang, J. X. Zhong, *Appl. Surf. Sci.* **2014**, *299*, 12.
[32] X. Wang, L. Yin, G. Liu, *Chem. Commun.* **2014**, *50*, 3460.
[33] R. Franco, M. I. Panayiotidis, J. A. Cidlowski, *J. Biol. Chem.* **2007**, *282*, 30452.
[34] F.-X. Xiao, J. Miao, B. Liu, *J. Am. Chem. Soc.* **2014**, *136*, 1559.
[35] Z. Yan, X. Yu, A. Han, P. Xu, P. Du, *J. Phys. Chem. C* **2014**, *118*, 22896.
[36] Q. Li, B. D. Guo, J. G. Yu, J. R. Ran, B. H. Zhang, H. J. Yan, J. R. Gong, *J. Am. Chem. Soc.* **2011**, *133*, 10878.
[37] Z. Chen, S. Q. Liu, M. Q. Yang, Y. J. Xu, *ACS Appl. Mater. Interfaces* **2013**, *5*, 4309.
[38] X. Y. Zhang, F. Xu, B. Q. Zhao, X. Ji, Y. W. Yao, D. P. Wu, Z. Y. Gao, K. Jiang, *Electrochim. Acta* **2014**, *133*, 615.
[39] I. V. Lightcap, T. H. Kosel, P. V. Kamat, *Nano Lett.* **2010**, *10*, 577.
[40] G. G. Huang, X. X. Han, M. K. Hossain, Y. Ozaki, *Anal. Chem.* **2009**, *81*, 5881.
[41] Y. Wang, J. Lu, L. H. Tang, H. X. Chang, J. H. Li, *Anal. Chem.* **2009**, *81*, 9710.
[42] G. Chen, J. Wang, C. Wu, C. Li, H. Jiang, X. Wang, *Langmuir* **2012**, *28*, 12393.
[43] R. Hong, G. Han, J. M. Fernandez, B. J. Kim, N. S. Forbes, V. M. Rotello, *J. Am. Chem. Soc.* **2006**, *128*, 1078.
[44] O. Akhavan, *Carbon* **2011**, *49*, 11.
[45] E. D. Spoerke, M. T. Lloyd, Y. J. Lee, T. N. Lambert, B. B. McKenzie, Y. B. Jiang, D. C. Olson, T. L. Sounart, J. W. P. Hsu, J. A. Voigt, *J. Phys. Chem. C* **2009**, *113*, 16329.

Received: July 9, 2015
Published online: November 30, 2015

